Bioelectrochemistry 80 (2011) 155–161

Contents lists available at ScienceDirect

Bioelectrochemistry

journal homepage: www.elsevier.com/locate/bioelechem

# Impedance spectroscopy and conductometric biosensing for probing catalase reaction with cyanide as ligand and inhibitor

Naima Bouyahia [a], Mohamed Larbi Hamlaoui [a], Mouna Hnaien [b], Florence Lagarde [b,*], Nicole Jaffrezic-Renault [b]

[a] Université de Annaba, Laboratoire LPCI, BP 12, El Hadjar, 23000 Annaba, Algeria
[b] Université de Lyon, LSA, UMR 5180 CNRS, Université Claude Bernard Lyon 1, 69622 Villeurbanne cedex, France

ARTICLE INFO

*Article history:*
Received 11 June 2010
Received in revised form 28 July 2010
Accepted 29 July 2010
Available online 14 August 2010

*Keywords:*
Cyanide
Catalase
Inhibition
Conductometric biosensor
Impedimetric biosensor
$I_{50}$

ABSTRACT

In this work, a new biosensor was prepared through immobilization of bovine liver catalase in a photoreticulated poly (vinyl alcohol) membrane at the surface of a conductometric transducer. This biosensor was used to study the kinetics of catalase–$H_2O_2$ reaction and its inhibition by cyanide. Immobilized catalase exhibited a Michaelis–Menten behaviour at low $H_2O_2$ concentrations (<100 mM) with apparent constant $K_M^{app} = 84 \pm 3$ mM and maximal initial velocity $V_M^{app} = 13.4$ µS $min^{-1}$. Inhibition by cyanide was found to be non-competitive and inhibition binding constant $K_i$ was 13.9 ± 0.3 µM. The decrease of the biosensor response by increasing cyanide concentration was linear up to 50 µM, with a cyanide detection limit of 6 µM. In parallel, electrochemical characteristics of the catalase/PVA biomembrane and its interaction with cyanide were studied by cyclic voltammetry and impedance spectroscopy. Addition of the biomembrane onto the gold electrodes induced a significant increase of the interfacial polarization resistance $R_p$. On the contrary, cyanide binding resulted in a decrease of Rp proportional to KCN concentration in the 4 to 50 µM range. Inhibition coefficient $I_{50}$ calculated by this powerful label-free and substrate-free technique (24.3 µM) was in good agreement with that determined from the substrate-dependent conductometric biosensor (24.9 µM).



## 1. Introduction

Cyanide is continuously released in small doses in the environment and is considered as a violent poison that constitutes a real hazard for aquatic ecosystems. It is naturally produced by certain bacteria, fungi, and algae and found in many foods and plants. Cyanide is also widely used in industry for the manufacture of synthetic fibers, plastics, as well as in electroplating baths and metal mining operations or as pesticide agent and intermediate in agricultural chemicals production [1,2].

The main toxic effects of cyanide are due to its high affinity to the iron atoms of haemoproteins such as cytochrome oxidase, peroxidase, ferric haemoglobin and myoglobin, as well as catalase (CAT) [3]. Many works have been carried out to understand the mechanism of interaction between cyanide and these enzymes. Processes involved as well as their kinetic and thermodynamic characteristics are variable. Eukaryotic peroxidase or CAT inhibition by cyanide proceeds via a rapid binding of the neutral form to the enzyme. Ferric ('met') haemoglobin and myoglobin react more slowly and bind to cyanide anion. Cytochrome oxidase, like peroxidase and CAT, binds to the neutral form but reacts very slowly in the resting state [4].

CAT, present in virtually all aerobic organisms and in many anaerobic organisms, is involved in the defence against oxidative damage. This enzyme dismutates hydrogen peroxide into water and oxygen in a two-step process [5]. Among the different CAT enzymes isolated and characterized, bovine liver CAT has shown useful applications in various industrial fields to remove hydrogen peroxide used as oxidizing, bleaching or sterilizing agent [6] and in the analytical field as a component of glucose [7] or hydrogen peroxide [8–11] biosensor systems. To improve the activity, stability and reusability of this enzyme, immobilization into or onto various materials including sol–gels [6], iron magnetic beads [12], synthetic or natural hydrogels [13–15], carbon nanotubes [9] or composite nanofibers [16] have been proposed. Immobilization can modify the protein conformation and thus change enzymatic activity. The most classical way to study the kinetics of $H_2O_2$ degradation by free or immobilized CAT consists in monitoring the decrease of $H_2O_2$ concentration during enzymatic reaction by UV spectroscopy. Nevertheless, the specificity, simplicity and inherent miniaturization afforded by the advances in modern electronics has enabled electrochemical sensors and microsystems to rival the most advanced optical methods for monitoring bioaffinity reactions [17]. To measure CAT affinity for $H_2O_2$, some authors have proposed to follow $0_2$ consumption by the free or immobilized enzyme by amperometry using a specific oxygen electrode [5,6,8]. Detection by cyclic voltammetry was also reported [10,11]. Recently, a very performing

* Corresponding author. Tel.: +33 472432627; fax: +33 472448319.
*E-mail address:* florence.lagarde@univ-lyon1.fr (F. Lagarde).

1567-5394/$ – see front matter © 2010 Elsevier B.V. All rights reserved.
doi:10.1016/j.bioelechem.2010.07.006

microfluidic system combined with electrochemical detection has been developed [18].

In this work, we propose to study $H_2O_2$ dismutation by CAT and inhibition of this reaction by cyanide by combining two complementary techniques. The first one is based on the determination of kinetics parameters of the enzymatic reaction using an original conductometric biosensor prepared by immobilizing CAT enzyme on the surface of interdigitated thin film electrodes. Conductometric mode of transduction offers many advantages compared to other electrochemical techniques as amperometry or voltammetry [19].

Kinetics informations will be further compared to cyanide-CAT binding data obtained by electrochemical impedance spectroscopy. This technique is a powerful tool for the label-free and substrate-free study of high affinity interactions. From fitting impedance data to appropriate equivalent electrical circuit, one can get specific characteristics of working electrode, in particular, properties of electrode/electrolyte interface that can be changed due to the formation of enzyme–inhibitor complex [20].

## 2. Experimental

### 2.1. Reagents

CAT enzyme (EC1.11.1.6, from bovine liver, 4540 U $mg^{-1}$ protein), bovine serum albumin (BSA), glycerol (99%), potassium hexacyanoferrate (III) ($K_3Fe(CN)_6$, >99%) and potassium hexacyanoferrate(II) ($K_4Fe(CN)_6 \cdot 3H_2O$, 98.5–102%) were provided by Sigma-Aldrich. Poly (vinyl alcohol) bearing photopolymerizable styrylpyridinium groups (PVA-SbQ) was purchased from Toyo Gosei (Shiba, Japan). Potassium cyanide (≥98%), acetone (99%), ethanol (96%), sulphuric acid (95–97%) and hydrogen peroxide (30% in water) were purchased from Fluka and used as reactants or for electrode pretreatment. $NaH_2PO_4$ (>99%) and $Na_2HPO_4 \cdot 12H_2O$ (>99%) were obtained from Sigma-Aldrich.

Buffer solution used for cyclic voltammetry and impedance measurements was Phosphate Buffer Saline (PBS) containing 140 mM NaCl, 2.7 mM KCl, 0.1 mM $Na_2HPO_4$ and 1.8 mM $KH_2PO_4$, adjusted to pH 7 with NaOH.

The reagents were used as purchased without any further pretreatment. All solutions were prepared using ultrapure water (resistivity > 18 MΩ cm) obtained from an ElgaStat UHQII purification system.

Since cyanide is a dangerous toxic compound, precautions must be taken to prevent any accidental release. A 10 mM stock solution was prepared in 0.01 mM sodium hydroxide and stored at 4 °C. It was used for the daily preparation of diluted working solutions.

### 2.2. Sensor design and enzyme immobilization

#### 2.2.1. Conductometric biosensor

The conductometric transducer used was fabricated at the Lashkaryov Institute of Semiconductor Physics (Kiev, Ukraine). It consisted of two identical pairs of gold interdigitated thin film electrodes (150 nm thick) built by gold vacuum deposition onto a ceramic substrate (5 × 30 mm). A 50 nm thick intermediate Cr layer was used to improve the adhesion of Au to the substrate. Both the digit width and interdigital distance were 20 μm, and their length was about 1.0 mm [19]. As a result, the sensitive area of each electrode was about 1 $mm^2$. The first pair of electrodes, covered by a non reactive BSA membrane, constituted the reference electrode. The second one, on which an enzymatic membrane containing both CAT and BSA was deposited, was the working pair of electrodes. The pads of the transducer were covered manually with BlocJelt acrylic varnish (ITW Spraytec, Asnières sur Seine, France) for their insulation.

To prepare the enzymatic biosensor, a two-step procedure was followed. 0.2 μL of a 20 mM phosphate buffer pH 7.2 containing 6% (m/v) BSA, 10% (m/v) glycerol and 4% of CAT was first deposited on the working pair of electrodes, while on the reference electrodes 0.2 μL of a mixture containing only 10% (m/v) BSA and 10% (m/v) glycerol was applied. In the second step of the procedure (enzymes immobilization), both pairs of electrodes were covered by 0.2 μL of a 10% (m/v) PVA-SbQ aqueous solution. PVA cross-linking was performed by irradiating the microelectrodes for 20 min at 365 nm in a Bio-link BLX UV-crosslinker (Vilbert Lourmat) equipped with five 8 W lamps.

Biosensors were used just after preparation or stored at 4 °C in a 20 mM phosphate buffer solution, pH 7.2 until measurements.

#### 2.2.2. Impedimetric biosensor

Gold substrates were provided by the Laboratoire d'Analyse et d'Architecture des Systèmes (LAAS, CNRS Toulouse). They were fabricated using standard silicon technologies. (100)-oriented, P-type (3–5 Ω cm) silicon wafers were thermally oxidized to grow an 800 nm-thick field oxide. Then, a 30 nm-thick titanium layer followed by a 300 nm thick gold top layer were deposited by evaporation under vacuum. Before use, gold electrodes were sonicated for 10 min in acetone, and then dried under nitrogen flow. After that, the gold surface was cleaned for 1 min with a freshly prepared "piranha" mixture ($H_2O_2$: $H_2SO_4$, 3:7, v/v) and rinsed carefully with large amounts of deionized water. Then plates were washed with ethanol, rinsed with water and finally dried under a nitrogen flow.

Modification of the gold electrodes was performed by successive deposition of CAT and PVA following the protocol already described for the conductometric electrodes.

### 2.3. Measurements

#### 2.3.1. Conductometric measurements

Microelectrodes were placed in a glass cell filled with 5 mL of a 5 mM phosphate buffer pH 7.2 under vigorous magnetic stirring. Measurements were then performed at 23 ± 2 °C by applying to the differential pairs of electrodes an alternating voltage (10 mV amplitude, 100 kHz frequency) generated by a low-frequency wave-form generator (SR830 Lock-in amplifier from Stanford Research Systems). These conditions allowed to reduce faradaic processes, double-layer charging and concentration polarization at the microelectrode surface. The response of the biosensor, corresponding to the evolution of conductance (G) after $H_2O_2$ addition, was recorded as a function of substrate concentration in the absence or in the presence of cyanide as enzyme inhibitor. For that, small aliquots (5–80 μL) of concentrated solutions containing $H_2O_2$ or a mixture of $H_2O_2$ and cyanide were added into the vessel after stabilization of the differential output signal in order to get final concentrations in the 0–300 mM range for $H_2O_2$ and 0–50 μM for cyanide. Initial rates of reaction were calculated from the first 30 s linear portion of the conductometric response versus time curve.

#### 2.3.2. Impedance and cyclic voltammetry measurements

Impedance measurements were performed in a 5 mL three-electrode electrochemical cell placed into a Faraday cage in order to improve the signal-to-noise ratio. A gold electrode (0.19 $cm^2$) modified with CAT and PVA was used as a working electrode, while a saturated calomel electrode (SCE) purchased from Radiometer Analytical (Villeurbanne, France) was used as a reference electrode. The auxiliary electrode was made of a platinum plate with an active surface of 0.385 $cm^2$. Working buffer was stirred magnetically.

Impedance measurements were performed using a Voltalab 80 instrument (Radiometer Analytical) controlled with VoltaMaster 4.0 software in the 100 mHz to 100 kHz frequency range, acquiring 5 points per decade. An excitation voltage of 10 mV was superimposed on a dc potential of −200 mV. Impedance data were fitted to equivalent electrical circuits by means of the ZView2 software (Scribner Associates, USA).

Cyclic voltammetry (CV) measurements were performed with the same equipment. The potential was cycled from −1 and 1 V (versus the reference electrode) with a scan speed of about 25 mV/s in PBS buffer containing 2 mM of $K_3Fe(CN)_6$ and $K_4Fe(CN)_6$. All electrochemical measurements were carried out at room temperature (20 ± 1 °C) in a Faraday cage.

## 3. Results and discussion

### 3.1. Preliminary characterization of the CAT/PVA biomembranes

Cyclic voltammograms (five first cycles) recorded for the $FE(CN)_6^{3-}$/ $FE(CN)_6^{4-}$ redox probe on a bare Au electrode and on the same electrode covered by the CAT/PVA biomembrane are presented in Fig. 1. Before membrane deposition, both oxidation and reduction peaks of the $Fe(CN)_6^{3-}$/$Fe(CN)_6^{4-}$couple were observed. The separation between anodic and cathodic peak potentials ($\Delta Ep = Ep(ox) - Ep(red) = 197$ mV) suggested a quite reversible process. After deposition, both peaks disappeared, which was attributed to the decrease of electron transfer through PVA membrane.

Total impedances of the bare and enzyme/PVA gold electrodes were also determined by varying frequency in the 100 mHz to 100 kHz range. The potential was repetitively cycled until two consecutive curves could be superimposed. It took about 7 min for the bare electrode, while 35 min were needed for the modified electrode. This result confirmed that electron transfer to the electrode was slowed down by the addition of the membrane. Nyquist curve of the bare electrode, presented in Fig. 2a, could be satisfactorily fitted with an equivalent electrical circuit which comprised the ohmic resistance of the bulk electrolyte ($R_s$) in series with a parallel combination of the constant phase element (CPE) as a non-ideal capacitor and the polarization resistance ($R_p$), representing interfacial resistance in the absence of any redox species (Fig. 2b). Due to surface heterogeneity, the impedance $Z(\omega)$ of such a nonideal layer can be expressed as $Z(\omega) = CPE^{-1}(j\omega)^{-n}$, where ω is a circular frequency and n parameter varies from 0 to 1. When n is close to 0, CPE is essentially a resistance. If n = 1, the CPE is a pure capacitance and electrode is considered as ideal [20].

On the contrary, Nyquist curve of the modified electrode could not be fitted using this simple model. The Randles–Ehrshler model, which includes Warburg impedance, $Z_w$, resulting from ion diffusion from the bulk electrolyte to the electrode interface, appeared as well suited (Fig. 2c). Fitting parameters obtained for bare and modified electrodes are presented in Table 1. n values are close to 1, suggesting that CPE can be more likely considered as a capacitive element. Membrane layer significantly affected CPE and $R_p$. A 1.3-fold decrease of CPE and a two-fold increase of Rp were observed. Belinova et al. reported much larger variations of these parameters (2-fold decrease of CPE and 5–6 increase of Rp) for butylcholinesterase (BuChE) immobilized on gold electrodes through cross-linking with glutaraldehyde [21]. This may be attributed to the swelling properties of PVA hydrogel, that results in a lower polarization resistance than GA-crosslinked BuChE film.

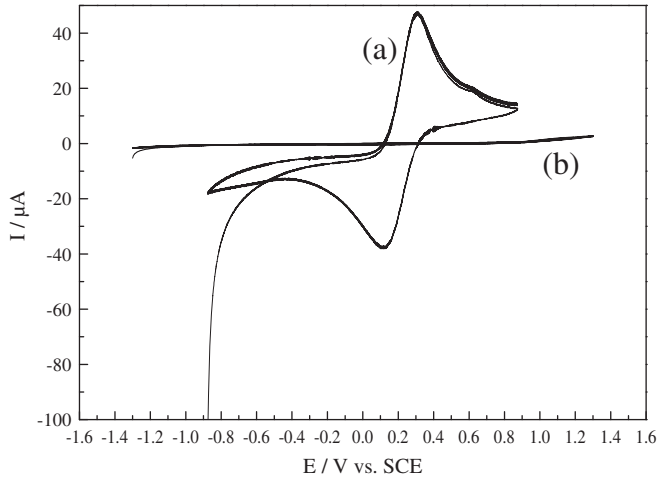


**Fig. 1.** The cyclic voltammograms of a 2 mM equimolar mixture of $FE(CN)_6^{3-}$ and $FE(CN)_6^{4-}$ recorded in phosphate buffer saline pH 7 at a bare gold electrode (a) and at the same electrode after catalase/PVA deposition (b). Scan rate: 25 mV $s^{-1}$ vs SCE.

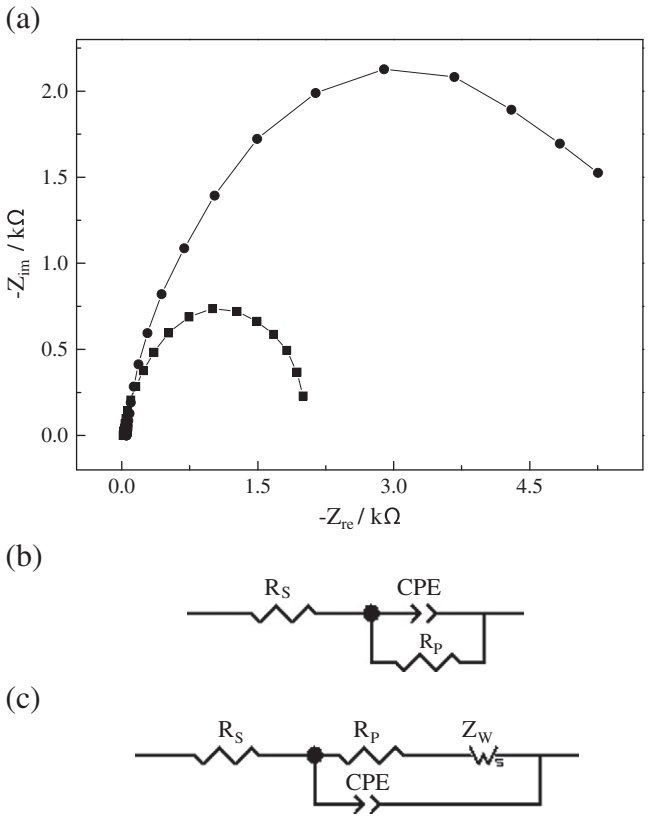


**Fig. 2.** Nyquist plots (a) of the complex impedance spectra of the gold electrode before (■) and after (●) catalase/PVA deposition. $Z_{im}$/kΩ represents the imaginary component and $Z_{re}$/kΩ the real component of the complex impedance $Z(\omega)$ calculated as the ratio between the system voltage phasor, $U(\omega)$, and the current phasor, $I(\omega)$, generated during the impedimetric measurements performed in phosphate buffer saline pH7 at −0.2 V vs SCE. Bare electrode data were modelled with the electrical equivalent circuit (b) and modified electrode data with circuit (c). Rs represents the ohmic resistance of the electrolyte solution, Rp the polarization resistance, $Z_W$ Warburg impedance and CPE the constant phase element.

### 3.2. Kinetic investigation of CAT–$H_2O_2$ reaction using the conductometric biosensor

#### 3.2.1. General characteristics of the biosensor in the absence of cyanide

The conductometric biosensor was first characterized by evaluating its response towards $H_2O_2$ in the absence of cyanide. As shown in Fig. 3, $H_2O_2$ degradation by CAT immobilized on the biosensor induced a rapid increase of conductance. A stable steady-state response, $G_{ss}$, was achieved in less than 5 min. The relationship between $G_{ss}$ and $H_2O_2$

**Table 1**
Values of equivalent circuit elements obtained by modeling the Nyquist curves presented in Fig.2. The best fit was achieved by minimizing the $\chi^2$ (khi square) parameter using the ZView2 software.

| Electrode | $R_s$/kΩ | CPE/µF(rad/s)$^{1-n}$ | n | $R_p$/kΩ | $\chi^2$ ($\times 10^{-4}$) |
|---|---|---|---|---|---|
| Bare Au | 0.062 | 11.1 | 0.9 | 2.0 | 9.7 |
| Catalase/PVA/AU | 0.186 | 8.7 | 0.85 | 4.12 | 5.4 |

concentration was examined in the 0–300 mM range. For that, eight standard solutions were used and five measurements were performed at each concentration level. The conductance increased linearly with $H_2O_2$ concentration up to 100 mM and a progressive saturation was observed beyond this value (Fig. 4). This linear domain is much wider than that of other CAT-based electrochemical biosensors reported before [8–10]. Coefficients of variation were between 0.5% and 1.6% in the linear domain, demonstrating the excellent intra-sensor repeatability of the method. Limit of detection was 6 μM (S/N = 3), slightly above literature values [8–10].

*3.2.2. Influence of cyanide on the kinetics of CAT reaction towards $H_2O_2$*

The conductometric biosensor was further used to study the kinetics of $H_2O_2$ degradation by immobilised CAT as well as the inhibitory effect of cyanide on this kinetics. It was assumed that the initial reaction rate $v_0 = -d[H_2O_2]/dt$ at t = 0 is proportional to $V_i = dG/dt$ at t = 0 and $V_i$ was deduced from the initial linear portion of the conductance versus time curve obtained at each substrate and inhibitor concentration.

For the first set of experiments, performed in absence of inhibitor, $H_2O_2$ concentration varied from 10 to 300 mM. As shown in Fig. 5, the plot $V_i$ vs $[H_2O_2]$ has an hyperbolic form, but only at low substrate concentrations (<100 mM), which seems to indicate that CAT, immobilised on the conductometric transducer, exhibits a Michaelis–Menten kinetics in a limited range of concentration. This result is coherent with kinetic data obtained in solution by Switala et al. [5].

To determine kinetic parameters and control that actually no cooperative effect occurs [22], experimental data were fitted with Michaelis–Menten equation (Eq. (1)) and Hill equation (Eq. (2)) in the 0–100 mM range:

$$V_i = \frac{V_{max}^{app}[H_2O_2]}{(K_M^{app} + [H_2O_2])} \quad (1)$$

$$V_i = \frac{V_{max}^{app}[H_2O_2]^n}{(K_M^n + [H_2O_2]^n)} \quad (2)$$

where $V_{max}^{app}$ and $K_M^{app}$ are the theoritical apparent Michaelis–Menten maximal reaction velocity and constant calculated from the data below 100 mM, while $K_H$ and n are the Hill constant and coefficient determined in the same conditions.

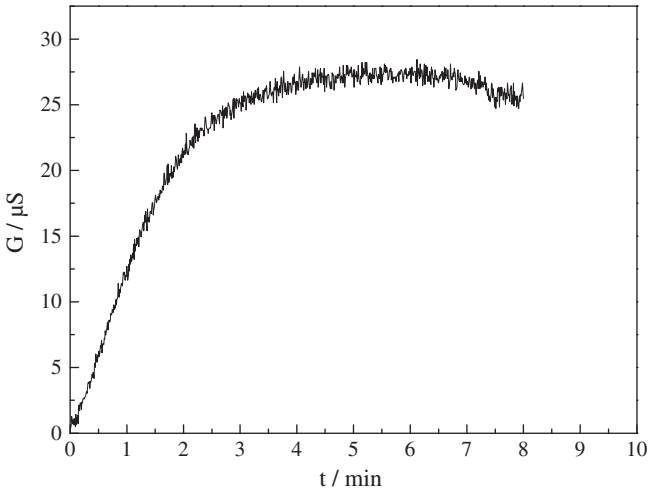


**Fig. 3.** Evolution of conductance G/μS as a function of time t/min after onset of reaction. $[H_2O_2] = 25$ mM. Measurements were performed in the absence of cyanide in 5 mM phosphate buffer pH = 7 and at T = 23 °C ± 2 °C. The slope of the initial linear portion of the curve ($V_i = dG/dt$ at t = 0) was calculated and assumed to be proportional to the initial rate of $H_2O_2$ disappearance.

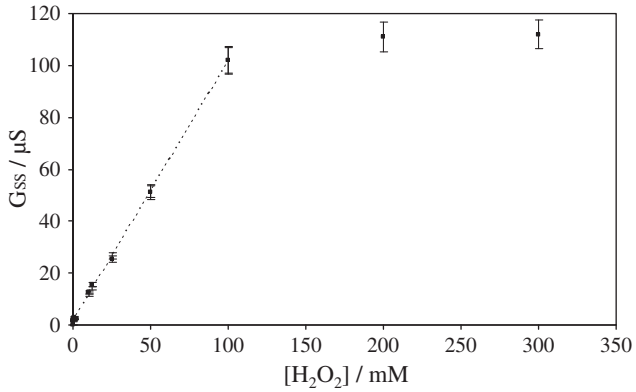


**Fig. 4.** Evolution of the steady-state conductance $G_{ss}$/μS as a function of $H_2O_2$ concentration $[H_2O_2]$/mM. Measurement conditions were the same as for Fig. 3. Values represent means ± standard deviations from 5 consecutive measurements. The dotted line corresponds to the regression of the linear part of the curve. Related equation is: $G_{ss}/\mu S = 1.00\ (\pm 0.08)\ [H_2O_2]/mM + 1.5\ (\pm 1.9)$ with r = 0.9992.

$V_{max}^{app}$ and $K_M^{app}$, can be experimentally determined from the slope and intercept of the double-reciprocal Lineweaver–Burk plot (Eq. (3)):

$$\frac{1}{V_i} = \frac{1}{V_{max}^{app}} + \frac{K_M^{app}}{V_{max}^{app}}[H_2O_2] \quad (3)$$

In the same way, n and $K_H$, can be drawn from the Hill plot (Eq. (4)):

$$\log\left(\frac{V_i}{V_{max}^{app} - V_i}\right) = n\log([H_2O_2]/M) - n\log(K_H/M) \quad (4)$$

As shown in Fig. 6 (full circles), Lineweaver–Burk plot was linear in the 0–100 mM range of substrate concentration. Calculated Michaelis–Menten parameters were $K_M^{app} = 85.3$ mM and $V_{max}^{app} = 13.4\ \mu S\ min^{-1}$. Hill plot was also linear in this concentration range ($R^2 = 0.995$), yielding a Hill coefficient of 0.98, close to 1, and a constant $K_H = 87.1$ mM. These results confirmed the absence of cooperativity and the Michaelis–Menten behaviour of immobilised bovine liver CAT below 100 mM $H_2O_2$.

For inhibition experiments, kinetic parameters were determined as a function of $H_2O_2$ concentration (10 to 100 mM) in the presence of 20, 30, 40 and 50 μM cyanide. In a general way, inhibitors can affect enzymatic reactions in a competitive, non-competitive or uncompetitive ways. Ogura

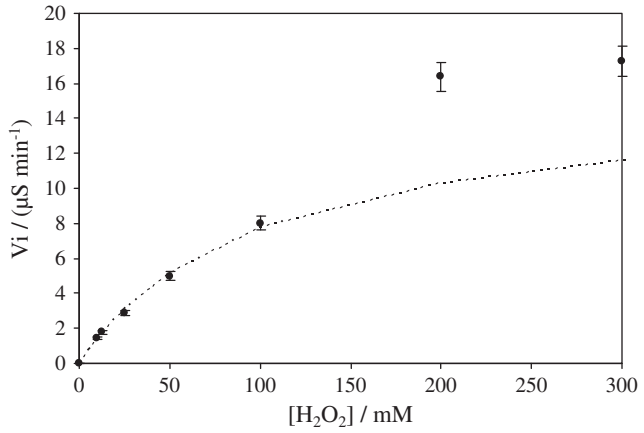


**Fig. 5.** Initial rate of reaction Vi/μS $min^{-1}$ as a function of $H_2O_2$ concentration/mM. Full circles represent experimental data (means ± standard deviations from 5 consecutive measurements) and dashed line recalculated curve after fitting (Eq. (2)). Measurement conditions were identical to that of Fig.3.

et al. suggested that cyanide acts as a non-competitive inhibitor of CATs at low $H_2O_2$ concentrations (<0.1 M) and becomes competitive only at higher concentrations [23]. A purely non-competitive inhibitor reacts with the enzyme-substrate complex, and slows down the rate of enzymatic reaction. In this case, and in the absence of cooperativity, the expression of initial velocity becomes Eq. (5):

$$V_i = \frac{V_{max}^{app}[H_2O_2]}{(K_M^{app}+[H_2O_2])} \times \frac{1}{\left(1+\frac{[KCN]}{K_i}\right)} \quad (5)$$

where $K_i$ represents the inhibition binding constant.

At a given substrate concentration, 1/Vi vs [I] (Dixon plot) is linear and converge on the x axis to a constant value ($-K_i$).

As shown in Fig. 6, Lineweaver–Burk plots of the initial velocities are linear in the 0–100 mM range of substrate concentration and converge on the x-axis, confirming that CAT follows Michaelis–Menten kinetics and that inhibition by cyanide is of a non-competitive type. $V_{max}^{app}$ was significantly affected by cyanide and decreased by a factor of about 6 by adding 50 μM KCN, while $K_M^{app}$ was quite constant. An average $K_M^{app}$ of 84 ± 3 mM was calculated. This value is not easily comparable to literature data which are obtained from free or immobilized commercial CAT of different declared activities using different methods and pH or temperature conditions (Tables 2 and 3). Han et al. [18], working on the same commercial bovine liver CAT, in similar measurement conditions (50 mM phosphate, pH 7.4, room temperature) reported a 62 mM Michaelis–Menten constant for the free enzyme. Entrapment of CAT in the PVA membrane of the biosensor induced only a 1.3-fold increase in the KM value. This small increase may be due either to conformational changes of the enzyme, resulting in a lower possibility of forming a substrate–enzyme complex, or to the lower accessibility of the substrate to the active sites of the immobilized enzyme caused by the increased diffusion limitation but at limited levels. Similar results involving change in $K_M$ and Vmax values of enzyme after immobilization have been already reported in literature. The discrepancy between free and immobilized CAT $K_M$ values strongly depends on the mode of immobilization chosen. As seen in Table 3, $K_M$ can decrease or increase after enzyme immobilization.

$1/V_i$ was also plotted against cyanide concentration at different concentrations of substrate (data not shown). The plots were linear and converged on the x-axis, confirming the non-competitive nature of the inhibition process. A mean apparent inhibition binding constant Ki was determined from the five Dixon plots: a value of 13.9 ± 0.3 μM, falling within the range of inhibitor concentrations used in the kinetic experiments, was obtained. This value is relatively close to that of Maj et al. ($K_i$ = 10 μM) determined for free CAT [4].

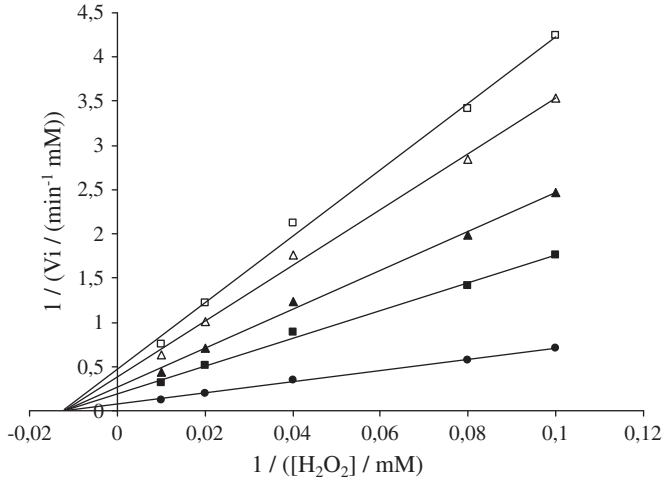


**Fig. 6.** The graphical determination of $K_M^{app}$ and $V_{max}^{app}$ from the double-reciprocal relationship Eq. (3) for [KCN]/μM = 0 (●), 20 (■), 30 (▲), 40 (△) and 50 (□). Measurement conditions were identical to that of Fig. 3.

**Table 2**
Influence of cyanide on the kinetic parameters of catalase–$H_2O_2$ reaction. $V_{max}^{app}$ and $K_M^{app}$ were calculated at each inhibitor concentration from the double-reciprocal plots of Fig. 6.

| [KCN]/μM | 0 | 20 | 30 | 40 | 50 |
|---|---|---|---|---|---|
| $V_{max}^{app}$/μS min$^{-1}$ | 13.4 | 5.2 | 4.0 | 2.8 | 2.2 |
| $K_M^{app}$/mM | 85.3 | 79.6 | 86.3 | 87.0 | 80.2 |

As presented in Fig. 7a, CAT activity towards $H_2O_2$, as measured with the conductometric biosensor, decreased linearly by increasing cyanide concentration up to 50 μM. The biosensor could thus be exploited as an inhibition-based biosensor for cyanide determination. A very low detection limit (6 μM) was obtained. Several enzymatic biosensors based on the inhibition of cytochrome oxidase [24], horseradish peroxidase [25,26] or tyrosinase [27–29] by cyanide and amperometric detection have been proposed in the literature. Only one biosensor based on CAT inhibition was reported [30]. Detection limit and linear range were 57 μM and 0.19–7.7 mM, respectively. The intra-sensor repeatability was also evaluated at three concentration levels from five consecutive measurements of the solutions using the same sensor. The variation coefficients were between 0.4% and 1.5% in the concentration range studied, demonstrating the very good repeatability of the cyanide biosensor response.

Finally, Fig.7a allowed to determine the inhibition coefficient $IC_{50}$ corresponding to the cyanide concentration inducing a 50% decrease of CAT activity. A 24.9 μM value was obtained.

### 3.3. Impedimetric investigation of the cyanide/CAT binding process

Impedimetric biosensor was used to study the formation of CAT-cyanide bioaffinity complex. Cyanide binding is expected to affect interfacial properties of the working electrode, inducing variations of resistance and capacitance of the equivalent circuit. The influence of cyanide addition on Nyquist diagrams of the Au/CAT/PVA electrode was investigated at different concentrations of inhibitor (15 to 100 μM). $R_s$, n and CPE values, obtained by fitting experimental data with the Randles–Ehrsler model (Fig. 2c), remained quite constant over the whole range of cyanide concentration. The absence of variation observed for CPE parameter may be explained by the small size and mass of cyanide compared to that of CAT. Membrane thickness is therefore not

**Table 3**
Influence of catalase immobilization on Michaelis–Menten $K_M$ constant.

| Mode of immobilization | Kinetics conditions | $K_M$/mM | | Ref. |
|---|---|---|---|---|
| | | Free catalase | Immobilized catalase | |
| – | 37 °C | 93 | – | [5] |
| – | Room temp. | 62 | – | [18] |
| Photoreticulated PVA coating | Room temp | n.d. | 84 | This work |
| Entrapment into sol–gels | 20 °C | 85.4 | 211 | [6] |
| Adsorption on magnetic beads | 25 °C | 22.8 | 32.6 | [12] |
| Adsorption on chitosan film | 25 °C | 25.2 | 27.7 | [13] |
| Adsorption on chitosan beads | 35 °C | 35 | 18 | [14] |
| Entrapment in synthetic hydrogels | 25 °C | 16.5 | 28.6 | [15] |
| Adsorption on carbon nanotubes | | n.d. | 1.7 | [9] |
| Entrapment into NiO particles | | n.d. | 0.96 | [11] |
| Covalent binding to PANCAA[a] | 25 °C | 34.07 | 77.9 | [16] |
| nanofibers PANCAA /MWCNT[b] nanofibers | | | 58.14 | [16] |

[a] PANCAA:poly(acrylonitrile-*co*-acrylic acid).
[b] MWCNT: multi-walled carbone nanotubes.

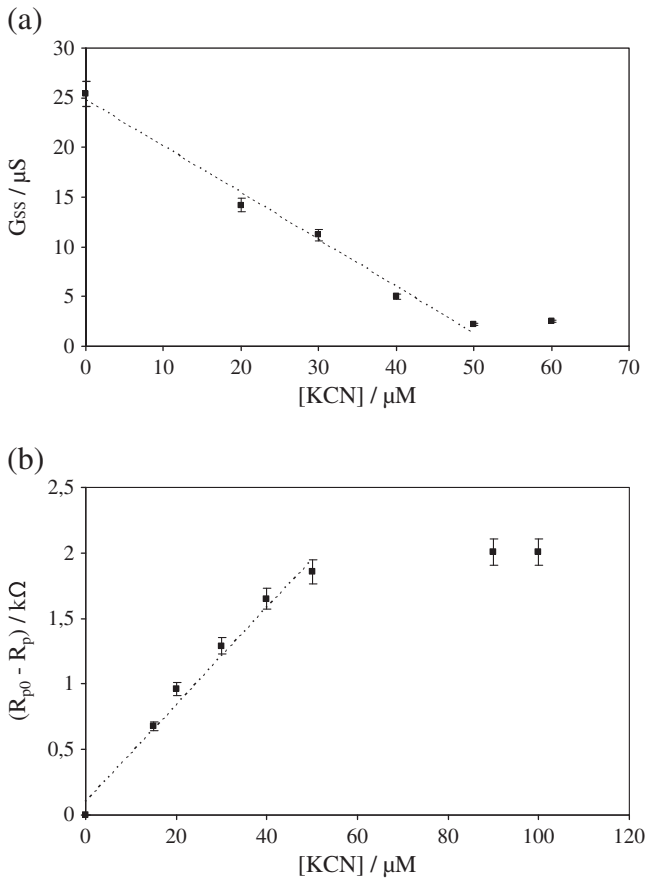


**Fig. 7.** Evolution of the steady-state conductance $G_{ss}$/µS (a) and the charge transfer resistance variation $Rp_0 - R_p$/_ (b) as a function of cyanide concentration [KCN]/µM. $G_{ss}$ was measured using the conductometric biosensor in experimental conditions described for Fig.3. $Rp_0$ and $R_p$ were deduced from impedimetric measurements performed in phosphate buffer saline pH7 at −0.2 V vs SCE. $Rp_0$ refers to $R_p$ for [KCN] = 0. Dotted lines correspond to the regression of the linear part of the curves. Related equations are: $G_{ss}/\mu S = -0.47\ (\pm 0.15)$ [KCN]/µM + 24.8 (±3.9) with r = 0.9879 and $(Rp_0 - Rp)/k\Omega = 0.037\ (\pm 0.007)$ [KCN]/µM + 0.10 (±.0.18) with r = 0.9813.

significantly modified by cyanide binding. Benilova et al. reported similar results for glycoalkaloids binding to butylcholinesterase [21]. On the contrary, a significant decrease of impedance, correlated to Rp diminution, occurred after cyanide addition. The decrease of Rp parameter may be attributed to the modification of enzyme conformation following cyanide binding process, inducing charge redistribution and/or conductance changes in the enzyme membrane.

As seen in Fig 7b, $Rp_0$–Rp increased linearly with cyanide concentration up to 50 µM. The minimal concentration of cyanide detectable by the bioaffinity sensor was 4 µM.

From this curve, it was also possible to calculate cyanide concentration yielding 50% of the maximal $Rp_0$–Rp value. This value (24.3 µM), corresponding to half the concentration of binding sites available for cyanide complexation, was very close to the concentration yielding a 50% decrease of CAT activity previously calculated with the conductometric biosensor (24.9 µM).

## 4. Conclusion

A conductometric biosensor based on CAT enzyme immobilized at the surface of interdigitated conductometric thin-film microelectrodes and covered with a PVA polymeric layer was developed for $H_2O_2$ determination. The biosensor response was rapid (<5 min), linear up to 100 mM and a detection limit of 50 µM was achieved. Using this biosensor, we showed that immobilized CAT exhibits a Michaelis–Menten behaviour at low $H_2O_2$ concentrations (<100 mM) with apparent constant $K_M^{app} = 84 \pm 3$ mM and maximal initial velocity $V_M^{app} = 13.4\ \mu S\ min^{-1}$. Inhibition by cyanide is non-competitive. The apparent inhibition binding constant $K_i$ was determined from the Dixon plots for different $H_2O_2$ concentrations and was 13.9 µM.

The possibility of nonfaradaic label-free and substrate-free impedance spectroscopy for probing affinity interactions between cyanide inhibitor and immobilized CAT was also demonstrated. The $I_{50}$ value of cyanide binding to CAT was 24.3 µM using this technique, very close to that measured by the biocatalytic conductometric biosensor (24.9 µM).

It was shown that conductometric and impedimetric responses depend linearly on cyanide concentration up to 50 µM with very good detection limits (6 and 4 µM, respectively), also demonstrating the great potential of these biosensors for quantitative analysis of cyanide.

## References

[1] D.A. Dzombak, Cyanide in Water and Soil, CRC Press LLC, New York, 2005 616 p.
[2] D.B. Donato, O. Nichols, H. Possingham, M. Moore, P.F. Ricci, B.N. Noller, A critical review of the effects of gold cyanide-bearing tailings solutions on wildlife, Environ. Int. 33 (2007) 974–984.
[3] D. Muniswamy, M. Vadingadu, H. Ramesh, R.M. Shambangouda, Impact of sodium cyanide on catalase activity in the freshwater exotic carp *Cyprinus carpio* (Linnaeus), Pest Biochem Physiol 92 (2008) 15–18.
[4] M. Maj, P. Nicholls, C. Obinger, A. Hillar, P.C. Loewen, Reaction of *E. coli* catalase HP11 with cyanide as ligand and as inhibitor, Biochim. Biophys. Acta 1298 (1996) 241–249.
[5] J. Switala, P.C. Loewen, Diversity of properties among catalases, Arch. Biochem. Biophys. 401 (2002) 145–154.
[6] D.L. Jurgen-Lohmann, R.L. Legge, Immobilization of bovine catalase in sol–gels, Enzym Microb Technol 39 (2006) 626–633.
[7] X. Gao, W. Yang, P. Pang, S. Liao, Q. Cai, K. Zeng, C.A. Grimes, A wireless magnetoelastic biosensor for rapid detection of glucose concentrations in urine samples, Sens Actuators B 128 (2007) 161–167.
[8] M.M.F. Choi, T.P. Yiu, Immobilization of beef liver catalase on eggshell membrane for fabrication of hydrogen peroxide biosensor, Enzym Microb Technol 34 (2004) 41–47.
[9] A. Salimi, A. Noorbakhsh, M. Ghadermarz, Direct electrochemistry and electrocatalytic activity of catalase incorporated onto multiwall carbon nanotubes-modified glassy carbon electrode, Anal. Biochem. 344 (2005) 16–24.
[10] J. Di, M. Zhang, K. Yao, S. Bi, Direct voltammetry of catalase immobilized on silica sol–gel and cysteine modified gold electrode and its application, Biosens. Bioelectron. 22 (2006) 247–252.
[11] A. Salimi, E. Sharifi, A. Noorbakhsh, S. Soltanian, Direct electrochemistry and electrocatalytic activity of catalase immobilized onto electrodeposited nano-scale islands of nickel oxide, Biophys. Chem. 125 (2007) 540–548.
[12] M. Sarı, S. Akgol, M. Karatasü, A. Denizli, Reversible immobilization of catalase by metal chelate affinity interaction on magnetic beads, Ind. Eng. Chem. Res. 45 (2006) 3036–3043.
[13] S.A. Cetinus, H.N. Oztop, Immobilization of catalase on chitosan film, Enzym Microb Technol 26 (2000) 497–501.
[14] S.A. Cetinus, H.N. Oztop, D. Saraydın, Immobilization of catalase onto chitosan and cibacron blue F3GA attached chitosan beads, Enzym Microb Technol 41 (2007) 447–454.
[15] M. Yakup Arıca, H. Avni Oktem, Z. Oktem, S. Ali Tuncel, Immobilization of catalase in poly(isopropylacrylamide-co-hydroxyethylmethacrylate) thermally reversible hydrogels, Polym. Int. 48 (1999) 879–884.
[16] Z.G. Wang, B.B. Ke, Z.K. Xu, Covalent Immobilization of redox enzyme on electrospun nonwoven poly(acrylonitrile-co-acrylic acid) nanofiber mesh filled with carbon nanotubes: a comprehensive study, Biotech. Bioeng. 97 (2007) 708–720.
[17] O.A. Sadik, A.O. Aluoch, A. Zhou, Status of biomolecular recognition using electrochemical techniques, Biosens. Bioelectron. 24 (2009) 2749–2765.
[18] Z. Han, W. Li, Y. Huang, B. Zheng, Measuring rapid enzymatic kinetics by electrochemical method in droplet-based microfluidic devices with pneumatic valves, Anal. Chem. 81 (2009) 5840–5845.
[19] N. Jaffrezic-Renault, S.V. Dzyadevych, Conductometric microbiosensors for environmental monitoring, Sensors 8 (2008) 2569–2588.
[20] E. Katz, I. Willner, Probing biomolecular interactions at conductive and semiconductive surfaces by impedance spectroscopy: routes to impedimetric immunosensors, DNA-sensors, and enzyme biosensors, Electroanalysis 15 (2003) 913–947.
[21] I.V. Benilova, A.P. Soldatkin, C. Martelet, N. Jaffrezic-Renault, Nonfaradaic impedance probing of potato glycoalkaloids interaction with butyrylcholinesterase immobilized onto gold electrode, Electroanalysis 18 (2006) 1950–1956.
[22] L. Acerenza, E. Mizraji, Cooperativity: a unified view, Biochim. Biophys. Acta 1339 (1997) 155–166.

[23] Y. Ogura, I. Yamazaki, Steady-state kinetics of the catalase reaction in the presence of cyanide, J Biochem (Tokyo) 94 (1983) 403–408.
[24] A. Amine, M. Alafandy, J.M. Kauffmann, M. Novak Pekli, Cyanide determination using an amperometric biosensor based on cytochrome oxidase inhibition, Anal. Chem. 67 (1995) 2822–2827.
[25] M.H. Smit, E.G. Cass, Cyanide detection using a substrate regenerating peroxidase-based biosensor, Anal. Chem. 62 (1990) 2429–2436.
[26] D. Shan, S. Cosnier, C. Mousty, HRP/[Zn–Cr–ABTS] redox clay-based biosensor: design and optimization of cyanide detection, Biosens. Bioelectron. 20 (2004) 390–396.
[27] M.H. Smit, G.A. Rechnitz, Toxin detection using a tyrosinase coupled oxygen electrode, Anal. Chem. 65 (1993) 380–385.
[28] J. Besombes, S. Cosnier, P. Labbe, G. Reverdy, A biosensor as warning device for the detection of cyanide, chlorophenols, atrazine and carbamate pesticides, Anal. Chim. Acta 311 (1995) 255–263.
[29] X. Hu, Z. Leng, Determination of cyanide using a tyrosinase amperometric biosensor with catechol as substrate, Analyst 120 (1995) 1555–1557.
[30] K. Stein, J.U. Hain, Catalase biosensor for the determination of hydrogen peroxide, fluoride and cyanide, Mikrochim. Acta 118 (1995) 93–101.